Contents lists available at ScienceDirect

Journal of Water Process Engineering

journal homepage: http://ees.elsevier.com

Modelling solute transport in water disinfection systems: Effects of temperature gradient on the hydraulic and disinfection efficiency of serpentine chlorine contact tanks

Danial Goodarzi [a], Soroush Abolfathi [b,*], Sina Borzooei [c]

[a] Department of Civil, Water and Environmental Engineering, Shahid Beheshti University, Tehran, Iran
[b] School of Engineering, The University of Warwick, Coventry, United Kingdom
[c] Department of Civil and Environmental Engineering, Politecnico di Torino, Torino, Italy

ARTICLE INFO

Keywords
Water treatment
Wastewater treatment
Baffled disinfection tank
Water disinfection
Temperature
RANS
Turbulence closure model
Residence time distributions
Advection-diffusion model

ABSTRACT

Chlorine residual plays a key role in determining the quality of treated water and wastewater. One of the most critical factors affecting chlorine decay rates is flow and ambient temperature. Detailed knowledge of temperature impacts on the efficiency and performance of chlorine contact tanks will enable optimum design and operation of water and wastewater treatment infrastructures. This paper develops a robust and computationally efficient three-dimensional numerical simulation model using Reynolds-averaged Navier-Stokes equations (RANS) with $k-\varepsilon$ turbulence closure model. A non-reactive tracer transport model is developed by implementing three-dimensional advection-diffusion equation. The Chlorine decay processes are simulated using Reynolds-averaged species transport model. Temperature effects on density and viscosity is simulated through Millero and, Poisson and Vogel equations, respectively. Eight scenarios with variation in inflow and ambient temperature are simulated in this study. The residence time distribution (RTD) and hydraulic efficiency indexes are determined for the simulation scenarios. It is shown that small fluctuation in inflow and ambient temperature cause a significant change in chlorine concentration and performance of disinfection tank. The analysis of numerical simulations indicated that increase in ambient and inflow temperature can increase chlorine decay by up to 75 %, leading to undesirable disinfection consequences and disruption of water treatment processes. The numerical model developed within this study was successfully validated against experimental measurements and it is shown to be robust and efficient tool to determine optimum inflow and ambient temperature configurations for high-efficiency water treatment processes and to prevent microorganism residual and by-products disinfection formation. The computational framework presented in this study can inform optimum design of water and wastewater treatment processes.

1. Introduction

In recent decades, industrialization and socioeconomic growth of nations have led to ever-increasing environmental pollution. The existence of solute and solid pollutants (i.e., microplastics, heavy metals) adversely impacting the quality of water resources [1]. Water and wastewater treatment facilities are under pressure to provide efficient treatment processes in accordance with water quality standards [2]. Optimizing design and operation of water treatment facilities are necessary to comply with tightening energy saving regulations as well as reducing the environmental impacts of these infrastructures [3].

The water disinfection is one of the most crucial processes of water and wastewater treatment, responsible for bacteria, viruses, and other pathogens inactivation [4]. Chlorine is widely being used as a disinfectant to prevent waterborne pathogens and comply with the international health standards. Effective and efficient water treatment processes are heavily relying on appropriate concentration of chlorine and sufficient contact time to inactivate infecting microorganisms. The concentration and decay rate of chlorine is influenced by chemical and environmental parameters including pH, temperature, water chemical composition and disinfectant type [5–8]. Hence, maintaining chlorine concentration in water treatment facilities at the levels suggested by water quality standards is a complex task to achieve, given all temporally varying environmental and chemical parameters influencing the decay rate of chlorine.

In recent years, due to tremendous improvements in computer hardware systems and parallel computing, there has been a growing interest in application of computational fluid dynamics modelling for understanding fate and mixing of pollutants in environmental systems [9,10] as well as investigating the effects of environmental variables on the efficiency and performance of water treatment infrastructures [10–13].

The computational fluid dynamic techniques used for modelling environmental problems can be fundamentally categorized into Eulerian grid-based [10–13] and Lagrangian particle-based (mesh-free) modelling techniques [11,13,14]. The Lagrangian modelling approaches are proven to be robust for those problems which undergo large deformations. However, Lagrangian modelling approaches are often associated with cumbersome and time-consuming computational efforts [68]. On the other hand, the application of Eulerian models for those problems with relatively small deformations, such as flow in wa-

* Corresponding author.
E-mail address: soroush.abolfathi@warwick.ac.uk (S. Abolfathi)

ter and wastewater treatment facilities, are proven to be both robust and computationally efficient [15,16].

One of the main aims of CFD modelling of disinfection processes within water treatment facilities is to understand chlorine decay processes under varying environmental and design conditions as well as improving the efficiency of the chlorine disinfection process. A comprehensive disinfection process simulation consists of four steps, including modelling flow, passive tracer transport, disinfectant reaction, and microorganism inactivation simulation. Several attempts have been made to investigate the hydraulic efficiency of disinfectant tanks through analysis of tracer dispersion and residence time distributions (RTD) curves. Undertaking pilot tracer measurements in water and wastewater treatment facilities is labor intensive and costly. Therefore, field-based measurements are not the desired and in some cases feasible option. Advancement in computational fluid dynamics (CFD) and parallel computing techniques have enabled robust and relatively cheaper numerical tracer simulation to investigate hydraulic efficiency of treatment tanks [17]. Previous studies have investigated the effects of the baffle, inlet, outlet, and geometry configurations on flow short-circuiting, the variance of RTD curves, and the hydraulic efficiency of the disinfectant tanks [18–21]. An early numerical simulation of contact tank was done by Wang et al. [22], confirming the reliability of $k-\varepsilon$ turbulence closure models in accurate prediction of flow parameters and hydrodynamic of chlorine contact tanks. The effects of baffle spacing on solute transport in contact tanks was investigated by Kim et al. [23], concluding that short distance between compartments of contact tank is essential to avoid severe flow short-circuiting.

Wols et al. [24] investigated geometrical orientations of baffles in chlorine contact tanks and recommended implementation of horizontal baffles and turning vanes for optimum design of contact tanks. Nasyrlayev et al. [25] investigated the effects of implementing perforated baffles to improve the mixing in disinfection tanks and reported reduction in dead zones in each compartment of the baffled contact tank. Carlston et al. [26] investigated the impact of inlet flow conditions and geometrical shapes on the hydraulic retention time of baffled tanks and highlighted the positive impact of tee-attachment installation at the inlet on retention time and hydraulic efficiency of contact tanks. Zhang et al. [27] successfully developed a numerical model for evaluating the efficiency of ozone contact tanks and concluded that fluctuations in seasonal flow rate has a significant impact on the performance of ozone disinfectant contact tanks.

Angeloudis et al. [28] adopted a combination of experimental and numerical investigations to study the impact of baffle configurations on the efficiency of chlorine contact tanks and concluded that improvement in hydraulic efficiency of the tank has a direct impact on improving bacteria and micro-organisms inactivation. Kizilaslan et al. [29] investigated the impacts of seasonal variations in the water supply on mixing and disinfection efficiency of the chlorine contact tank and reported significant effects of temporal variations of flow conditions on pathogen inactivation and chlorine concentrations. The effects of flow unsteadiness and large-scale turbulent flow structures on scalar transport was investigated by Ouro et al. [30] and Zhang et al. [31] using high resolution turbulence models (i.e., Large Eddy Simulation) [30,31]. Long et al. [32] developed a CFD model to simulate a UV disinfectant tank and demonstrated the ability of CFD models to predict flow, radiation intensity, and concentration of microorganisms in UV reactors.

Fisher et al. [33] experimental investigations highlighted the significant role of temperature fluctuations in the chlorine decay rate. Ambient and seasonal variations in temperature cause a notable increase in chlorine concentration decay rate. For an average rise of 5 °C temperature, the chlorine decay rate was reported to increase by two folds [34]. Optimizing efficiency of chlorine contact process will have direct impact on the overall energy performance of water and wastewater treatment processes [69]. Despite the significance of temperature variations on the performance of chlorine disinfection tank, there is no robust computational framework to inform the design and optimum operations of disinfection processes by modelling the combined effects of flow conditions, temperature fluctuations, density and viscosity variations, solute transport and chemical reactions. This paper develops a computationally robust numerical model to investigate the effects of temperature fluctuations on the solute transport and performance of chlorine contact tank. The temperature effects on density and viscosity are modeled based on empirical equations of Millero and, Poisson and Vogel, respectively. This study will develop a non-reactive tracer transport model to simulate tracer transport and dispersion in the numerical baffled contact tank. The chlorine decay processes across the contact tank is computed by the Reynolds-averaged species transport model. The numerical model developed in this study is successfully validated against laboratory-based tracer measurements from a serpentine chlorine contact tank. Eight simulations scenarios are performed to investigate temperature effects on the performance of a serpentine chlorine contact tank. The simulation results show that numerical model developed in this study can be used as robust tool for optimized design and implementation of baffle chlorine contact tanks.

2. Method

2.1. Computational domain and boundary conditions

This study develops a numerical simulation tool comprising of flow hydrodynamic, solute and chlorine transport models in a three-dimensional (3D) Cartesian coordinate system to investigate the effects of temperature variations on the performance of a baffled chlorine disinfection tank. The computational domain, geometry of the tank, boundary conditions (Table 1) and computational scenarios (Table 4) are designed based on the experimental study described by Angeloudis et al. [28]. The numerical laboratory-scale disinfection tank is 3.0 m long, 2.0 m wide and 1.02 m deep (Fig. 1). The tank is consisted of eight segments of equal size demonstrating a typical standard serpentine contact tank which is broadly utilized in water and wastewater treatment plants [4,35]. The nominal hydraulic retention time of the tank is 21.11 min (flow rate = 0.00472 m^3/s) and the total volume of the tank after reducing the volume occupied by inner walls is 5.98 m^3, across all the simulation scenarios. The inlet and outlet boundaries are located at the top of the tank, on the left and right sides, respectively (see Fig. 1). The inlet width is equal to a compartment's width and the height is approximately one-fourth of the tank depth (further details on the tank geometry are given in Angeloudis et al. [28]).

Table 1
Summary of the boundary conditions used in this study.

Boundary conditions				
Variable	Inlet	Outlet	Top	Walls and bottom
Velocity	fixedValue	inletOutlet	symmetryPlane	No-slip
Pressure	zeroGradient	fixedValue	symmetryPlane	zeroGradient
Turbulent kinetic energy (*k*)	fixedValue	inletOutlet	symmetryPlane	kqRWallFunction
Turbulent energy dissipation (ε)	fixedValue	inletOutlet	symmetryPlane	epsilonWallFunction
υ_t	calculated	inletOutlet	symmetryPlane	nutkWallFunction
Temperature	fixedValue	calculated	zeroGradient	fixedValue
Chlorine	fixedValue	calculated	zeroGradient	zeroGradient
Passive scalar	uniformFixedValue	calculated	zeroGradient	zeroGradient

Table 4
Simulation scenarios.

No.	Case	Temperature (Centigrade)		Flow rate (lit/sec)	Tank dimension (m)			Volume (m^3)	HRT_N (min)
		Inlet	Ambient		Length	Width	Height		
1	**15C**	15	15	4.72	3	2	1.02	5.98	21.11
2	**20C**	20	20						
3	**25C**	25	25						
4	**30C**	30	30						
5	**2.5A-20C**	20	22.5						
6	**(-2.5)A-20C**	20	17.5						
7	**1A-20C**	20	21						
8	**(-1)A-20C**	20	19						

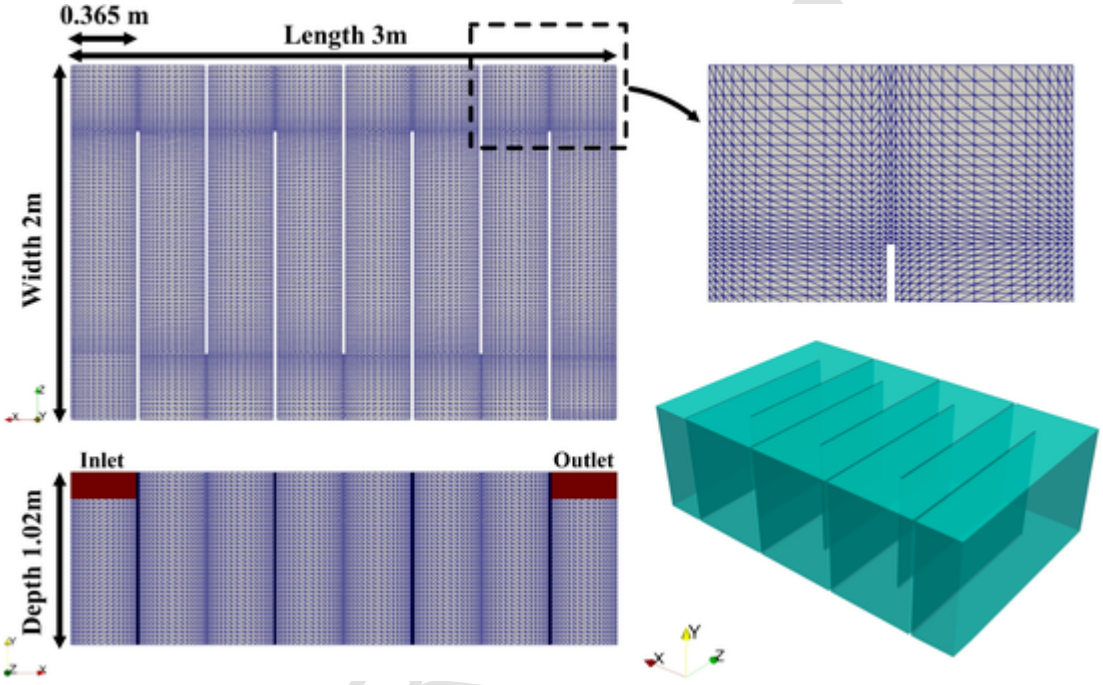

Fig. 1. Schematic of serpentine chlorine contact tank and the numerical mesh.

To begin the numerical simulation, the zero initial conditions for velocity and pressure inside the tank were set, although, kinematic energy and turbulent kinetic energy (k) and turbulent energy dissipation (ε) are estimated based on inflow condition [36,37]. The inlet and outlet boundary conditions are set as velocity-inlet and pressure-outlet with a constant flow-rate. No-slip wall boundary condition is considered for surrounding, baffled walls, and bottom of the tank. Table 1 summarizes the boundary conditions adopted in this study.

The numerical domain is discretized using a structured mesh technique along with a mesh refinement algorithm near the walls, and consists of 484,580 hexahedron cells. Flow variables are significantly affected by the presence of tank baffle and walls, where the viscosity gradient is large in the calculation of turbulent flow variables. Therefore, a careful treatment of near-wall region is essential to ensure accurate and robust calculation of wall-bounded turbulent flows. The k-ε turbulence closure model used in this study is capable of implementing empirical wall functions to model the flow and solute transport near the walls. Adoption of these wall functions enable connecting the internal area between the wall and the fully developed turbulent region [38]. Hence, resolving viscous sub-layer, which significantly increase computational costs, was not required for this study [38,39]. The distance to the wall modeled by the wall function is divided into three regions of viscous sub-layer ($0 < y+ < 5$), the buffer layer ($5 < y+ < 30$) and the Log layer ($30 < y+ < 200$) [40] and defined as:

$$y^+ = \frac{y \times u_\tau}{\upsilon} \tag{1}$$

$$u_\tau = \sqrt{\frac{\tau_\omega}{\rho}} \tag{2}$$

where y^+ is the dimensionless distance from the wall, u_τ represents the friction velocity, τ_ω denotes the wall shear stress [kg/m·s^2], ρ and υ are density [kg/m^3] and kinematic viscosity [m^2/s], respectively. The value of y + for the first computational cell is essential, as it determines where the first cell is located. The dimensionless velocity is defined as:

$$u^+ = \frac{u}{u_\tau} \tag{3}$$

To accurately solve the near wall region, the first cell center located at the wall should lie in the logarithmic layer, where turbulence dominates over vis-

cous effect and velocity profile is logarithmically shaped [41,42] defined by Eq.4:

$$u^+ = \frac{1}{\kappa} ln(y^+) + 5.2 \tag{4}$$

where $\kappa = 0.41$ is the Karman constant [39,43]. In this study, all the first cells near the walls are kept in the Log layer and the y + values are ranging from 30 to 50 to maximize computational accuracy.

2.2. Mathematical modelling and governing equations

Reynolds averaged Navier–Stokes (RANS) equations are used as the governing equations for fluid motion.

$$\frac{\partial \rho}{\partial t} + \nabla . \rho u = 0 \tag{5}$$

$$\frac{\partial}{\partial t} \rho u = -(\nabla . \rho u u) - \nabla p - \nabla . \tau + \rho g \tag{6}$$

where ρ is density [kg/m^3], u denotes average velocity [m/s], t is time [s], τ denotes stress sensor [N/m^2], p is pressure [kg/ms^2] and g represents the gravitational body force [m/s^2]. Finite Volume numerical scheme is utilized to develop the three-dimensional flow, heat and chlorine transport models. Eddy viscosity term in the RANS equations is solved by adopting k-ε turbulence closure model [44]. The numerical accuracy and robustness of the k-ε turbulence closure model used in this study was confirmed by related literature [28,29,35,45,46]. The turbulent viscosity μ_t, is computed according to Eq.7:

$$\mu_t = \rho C_\mu \frac{k^2}{\varepsilon} \tag{7}$$

where C_μ is set to 0.09, k is turbulent kinetic energy, and ε is the dissipation rate of turbulent kinetic energy. The thermal diffusivity k_t, is computed as a function of Prandtl number Pr_t, C_p is specific heat capacity and μ_t as Eq.8:

$$k_t = \frac{C_p \mu_t}{Pr_t} \tag{8}$$

The procedures to compute the turbulent kinetic energy k, and turbulent energy dissipation ε, are described in Eq. 9 and 10, respectively:

$$\frac{\partial}{\partial t}(\rho k) + \nabla . (\rho u k) = \nabla . \left(\left(\mu + \frac{\mu_t}{\sigma_k} \right) \nabla k \right) + P_k - \rho \varepsilon \tag{9}$$

$$\frac{\partial}{\partial t}(\rho \varepsilon) + \nabla . (\rho u \varepsilon) = \nabla . \left(\left(\mu + \frac{\mu_t}{\sigma_\varepsilon} \right) \nabla \varepsilon \right) + C_{\varepsilon 1} \frac{\varepsilon}{k} P_k - C_{\varepsilon 2} \rho \frac{\varepsilon^2}{k} \tag{10}$$

where P_k denotes production rate of turbulent energy. The numerical constants used for computing turbulent kinetic energy and turbulent energy dissipation are shown in Table 2:

Table 2
Numerical constants for the $k-\varepsilon$ turbulence model.

Numerical constant	Value
$C_{\varepsilon 1}$	1.44
$C_{\varepsilon 2}$	1.92
C_μ	0.09
σ_k	1
σ_ε	1.3
Pr_t	0.9

2.3. Temperature effects on density and viscosity

Flow temperature fluctuations can change fluid properties such as density and pressure which can influence the water and wastewater treatment processes. The impact of temperature on the flow pressure distribution within the chlorine contact tank is negligible and hence this study adopts a constant pressure approach for temperature fluctuations. However, the inflow and ambient temperature difference can introduce stratification and change the density of water throughout the chlorine contact tank. Previous experimental and numerical research of Hendi et al. and Goodarzi et al. hypothesize that even small variations in effluent density throughout the water and wastewater treatment processes could have significant impacts on the performance and efficiency of water treatment strategies and could alter flow condition from the desired hydraulic conditions [47,48]. This study numerically investigates the extend of influence of temperature induced density fluctuations and quantify the relationship between water density and temperature variations using Millero and Poisson (1981) numerical procedures according to Eq. 11 [49]:

$$\begin{aligned} \rho_t = {} & 999.842594 + 6.793952 \times 10^{-2} T \\ & - 9.095290 \times 10^{-3} T^2 + 1.001685 \times 10^{-4} T^3 \\ & - 1.120083 \times 10^{-6} T^4 + 6.536336 \times 10^{-9} T^5 \end{aligned} \tag{11}$$

where ρ_t denotes density as a function of temperature [kg/m^3] and T is temperature [°C].

The flow temperature and the shear effects are the main contributing factors influencing the viscosity of the fluid (effluent) in the water treatment process. Given that the fluid in the disinfection tank is Newtonian (water), viscosity is not altered by the shear rate, and it is only a function of temperature variations. This study adopts Vogel's model to numerically model the impact of temperature variations on the flow viscosity. The temperature-based viscosity model follows Eq. 12 [50]:

$$\upsilon = \exp(A + \frac{B}{(T + 273.15) + C}) \times 10^{-6} \tag{12}$$

where ν_t is kinematic viscosity [m^2/s], T denotes temperature [°C], and the experimental constant are taken as $A = -3.7188$, B = 578.919 and C = −137.546 [50].

2.4. Solute transport modelling

A non-reactive tracer transport model is developed by implementing advection-diffusion equation to simulate tracer transport in the baffled chlorine tank. The hydraulic efficiency parameters including real hydraulic retention time and short-circuiting are determined from residence time distributions (RTD) curves generated from tracer simulation data. To capture residence time characteristics, a passive scalar, with concentration of $s = 1$ [Unit mass/m3], is injected at the inlet boundary of the numerical domain and, the temporal variations of concentration are measured within the tank and at the outlet boundaries. Tracer modelling was conducted using the dynamic simulation method, which continued with the computation of the advection-diffusion equation, once the flow in the baffled contact tank was reached a steady-state condition [51]. Transport of the passive scalar is governed by the three-dimensional advection-diffusion equation described by Eq. 13 [43]:

$$\frac{\partial s}{\partial t} + \upsilon . \nabla s = \nabla \left[\nabla \left(D + D_t \right) s \right] \tag{13}$$

where s [Unit mass/m^3] denotes tracer concentration, D and D_t represent the molecular diffusion coefficient and the turbulent molecular diffusion coefficient [m^2/s], respectively.

In the previous numerical studies, sensitivity analysis indicated the impact of turbulent Schmidt number on the hydraulic efficiency indexes derived from the numerical model through the RTD curves [52]. To this date there is no generally accepted value of turbulent Schmidt number for modelling effluent flows in water disinfection tanks. Determination of the value of Schmidt number

for simulation is heavily dependent on the geometry of the water tank and flow-geometry interactions [53]. According to sensitivity analysis carried out for this study and in accordance with the similar numerical studies, $Sc_t = 1$ was selected as the most suitable value of turbulent Schmidt number for simulating flow in the baffled chlorine contact tank [52,54,55]. The Real Hydraulic Retention Time (HRT_R) and variance are calculated by instantaneous measurement of passive scalar concentration at the outlet boundary using Eq. 14:

$$HRT_R = \frac{\int_0^\infty ts\,(t)\,dt}{\int_0^\infty s\,(t)\,dt} \tag{14}$$

In reality, the hydraulic retention time is not equal to the nominal hydraulic retention time of the process tanks and the actual hydraulic retention time is always less than nominal hydraulic retention time [56]. The effective volume index *e*, describes the available volume percentage from the total volume of the tank in which the fluid pass through [57], directly influencing the efficiency and effectiveness of chlorine disinfection process. An optimal design of disinfection tanks lead into higher effective volume and improved process efficiency, respectively. The effective volume of the serpentine chlorine tank (Eq. 15) is determined as the ratio of the real hydraulic retention time (HRT_R) to the nominal hydraulic retention time (HRT_N) [58]:

$$e = \frac{HRT_R}{HRT_N} \tag{15}$$

Further hydraulic efficiency indexes, including short-circuiting (t_{10}), mixing M_o, θ_{10}, θ_p, θ_{90}, which were used to evaluate the numerical model are described in Table 3 [19,59,60]:

The short-circuiting index provides information about the volume of the fluid (effluent) which leave the tank earlier than the nominal hydraulic retention time, this phenomena is derived and governed by advection of the fluid. The mixing index shows the random walk type propagation and transport of the fluid throughout the tank. The mixing is governed by the turbulent diffusion processes and is influenced by flow characteristics that can influence the propagation and transport (i.e. recirculation and dead zones). The hydraulic efficiency indexes used for evaluating the numerical results are further elaborated by Teixeira et al. [59] and Demirel et al. [19].

2.5. Chlorine decay

Chemical species transport and reaction are computed using the Reynolds-averaged species transport equation described by Eq. 16:

$$\frac{\partial C}{\partial t} + \upsilon.\nabla \mathrm{C} - \nabla\left[\nabla\left(D + D_t\right) C\right] = S_p \tag{16}$$

where averaged concentration of chlorine is denoted by C [Unit mass/m^3], averaged chemical reaction of chlorine is implemented as a source term in Eq. 16 [43]. The dynamic simulation method was adopted to simulate flow hydrodynamic for the duration of four times the nominal hydraulic retention time (to reach steady-state condition). The chlorine transport and decay were simulated by introducing a constant initial chlorine concentration of 2 mg/l for all simulation cases. The spatially averaged concentrations of chlorine at the outlet boundaries were determined for every 25 s of the simulation.

Table 3
Hydraulic efficiency indexes.

Index	Definition
$\theta_{10} = \frac{t_{10}}{\tau}$	Time of tracer mass reaching above of 10 % at the outlet
$\theta_p = \frac{t_p}{\tau}$	Time of the peak concentration
$\theta_{90} = \frac{t_{90}}{\tau}$	Time of tracer mass reaching above of 90 % at the outlet
$Mo = \frac{t_{90}}{t_{10}}$	Morrill index (Mo)

Process of chlorine decay is influenced by the chemical reaction of chlorine with both organic and inorganic substances in the tank. Brown et al. [8] demonstrated that the chlorine decay process in the disinfectant tank includes a rapid intense phase and a slower phase. The rapid intense decay phase is responsible for a reduction of about 37–53 % of the chlorine concentration [61]. Thus, this study utilized a parallel second-order model, which is capable of simulating chlorine concentration decay due to a combination of the fast and slow decay phases. The chlorine decay rate is described and simulated based on Eq. 17 [28,35,62]:

$$\frac{\partial C_{Cl}}{\partial t} = \frac{\partial C_F}{\partial t} + \frac{\partial C_s}{\partial t} = -K_F C_F C_{Cl} - K_S C_S C_{Cl} \tag{17}$$

where C_{Cl} is the chlorine concentration [mg/L], K_F and C_F denote reaction rate coefficients [L/(mgCl.h)] and concentrations [mgCl-equiv/L] for fast phase, respectively, K_S and C_S describe reaction rate coefficients and concentrations of the slow decay phase, respectively.

Chemical reaction rate coefficients are computed as a function of temperature, described by Arrhenius empirical equation:

$$K = Ae^{\left(\frac{E_A}{RT}\right)} \tag{18}$$

where K is the reaction-rate coefficient, R is the ideal gas constant [= 8.31 J/(mol.K)], A and E_A are the frequency factor and activation energy, respectively.

Theoretically, the value of the minimum energy to initiate the reaction E_A, reflects sensitivities of reaction rates to temperature variations. Previous studies have confirmed the accuracy and robustness of the Arrhenius equation to determine temperature effects on the chlorine decay coefficient [6,63,64]. The temperature effects on the fast and slow reaction-rate coefficients are investigated by Fisher et al. [65] and suggested an improved equation based on the Arrhenius empirical relation as follows [28,33,62,65,66]:

$$\begin{aligned}\frac{\partial C_{Cl}}{\partial t} = &-K_F e^{\left(\frac{\frac{-E_A}{R(20-T)}}{(273+T_0)(273+T)}\right)} C_F C_{Cl} \\ &- K_S e^{\left(\frac{\frac{-E_A}{R(20-T)}}{(273+T_0)(273+T)}\right)} C_S C_{Cl}\end{aligned} \tag{19}$$

The experimental coefficients of K_F and K_S in Eq. 19 are taken as 2.77×10^{-4} [1/s] and 4 × 10–3 [1/s], respectively, in accordance with Angeloudis et al. [28] measurements.

2.6. Model validation and verification

The numerical model described and developed in this study was implemented in OpenFOAM. The numerical scenarios were simulated on a high-performance computing facility using 32 computational nodes. The total simulation time of ~1152 CPU hours (36 h real-time) was dedicated to perform simulations for each case.

The model developed in this study solves the governing equations of flow hydrodynamics and chlorine transport by using the Semi-Implicit Method for Pressure-Linked Equations. The computational algorithm uses a combination of Pressure Implicit with Splitting of Operator and Semi-Implicit numerical techniques for Pressure-Linked Equations methods. The temperature effects on density and viscosity are implemented to the numerical code by solving Eq. 11 and 12, for each computational time-step.

For all simulation scenarios (summarized in Table 4), flow hydrodynamics equations are computed for a simulation time of four times greater than the nominal hydraulic retention time of the baffled contact tank, until the steady-state condition is reached for the fluid flow (water) in the chlorine tank. The dynamic simulation method is implemented to compute flow hydrodynamic, chlorine concentration, temperature transfer, density, viscosity and chlorine transport and decay simultaneously at every time-step.

The numerical model developed within this study is validated by comparing the result of tracer simulations to the experimental measurements of An-

geloudis et al. [35]. The grid-independency study was performed with four meshing of varying resolutions, including 260k, 380k, 480k and 500k hexahedron elements (namely Mesh 1–4, respectively). The retention time distribution curve is determined from the numerical results for each meshing, by solving the mass transport equation and studying the numerical tracer concentration at the outlet [28,35,67].

Fig. 2 illustrates the normalized cumulative RTD curves of the tracer at the outlet and compares the numerical results for different mesh resolutions with the experimental measurements of Angeloudis et al. (2014) [15]. The normalized concentration of the tracer is defined as $s(\theta) = \frac{s}{s_0}$ where θ is normalized time defined as $\theta = \frac{t}{T}$. The comparison between the numerical simulations and experimental measurements indicates that the model developed in this study is successfully validated and is capable of reproducing laboratory measurements.

Further validation of the numerical model is performed by comparing the normalized numerical vertical velocity at the center of compartments 1, 2 and 8 with the experimental measurements (Fig. 3). The velocity is normalized with use of the bulk velocity, U_b, taken as 0.015 m.s^{-1}. Positive velocity values in Fig. 3 show the velocity in stream wise direction. The comparison between numerical velocity profiles with Angeloudis et al. (2014) data show that in general the developed model is in good agreement with the measurements.

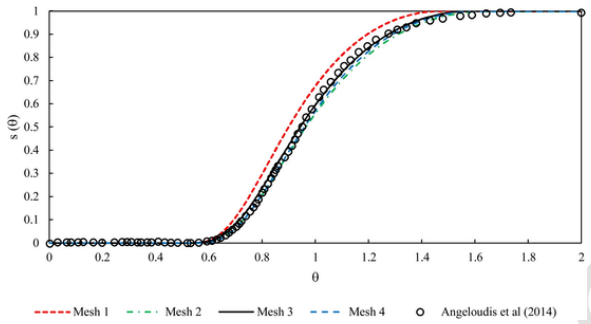

Fig. 2. Comparison of numerically derived normalized cumulative RTD curves with Angeloudis et al. (2014) measurements.

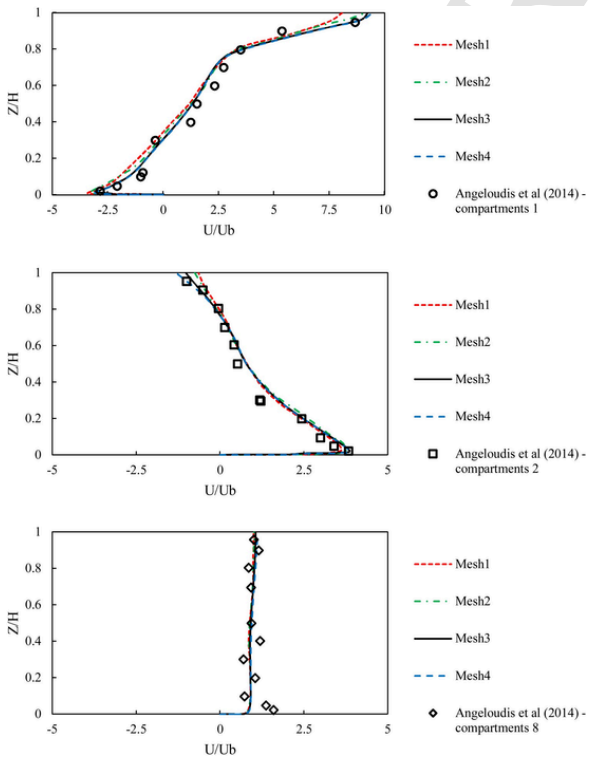

Fig. 3. Comparison of normalized numerical vertical velocity profiles at compartments 1, 2 and 8 with the experimental measurements of Angeloudis et al. (2014).

The comparison of solute transport in contact tank using different turbulence models such as RANS and LES models (e.g., Zhang et al. [31] and Ouro et al. [30]) showed slight effects of flow unsteadiness on scalar dispersion. Despite RANS models can fail to accurately resolve flow structure with anisotropic turbulence and large-scale flow structures, for the case of flow in serpentine chlorine contact tank in this study, time-averaged flow properties (quasi-steady flow, short-circuiting and dead zones) are well-described by RANS equations along with $k-\varepsilon$ turbulence closure model, resulting to robust and accurate prediction of hydraulic efficiency of the tank.

Fig. 3 indicates that Mesh number 3 and 4 have better performance in comparison to other meshing resolutions. For numerical accuracy and robustness, as well as computational efficiency, this study uses Mesh 3 (480k hexahedron elements) for simulating all the test cases described in Table 4.

2.7. Simulation scenarios

The impact of temperature gradient flow on the performance of a baffled chlorine contact tank is comprehensively investigated through eight simulation scenarios. The scenarios are designed to capture variation in inflow and ambient temperature. Inflow temperature effects are assessed using four simulation scenarios with a varying water temperature of 15, 20, 25 and 30 °C, which represent a typical range of inflow water temperature in water treatment plants. Furthermore, four simulation scenarios are dedicated to understand the effect of temperature difference between inflow with the temperature of 20 °C and the ambient (at +2.5, +1, -2.5 and -1 °C from inflow) and. The computational scenarios are designed to investigate the impact of the ambient flow of higher and lower temperatures than inflow, on the performance of the baffled chlorine contact tank (Fig. 1). Table 4 summarizes the simulation scenarios. Positive and negative notations for simulation scenarios denote higher and lower ambient temperature than water inflow temperature, respectively. Fixed temperature is set as a boundary condition for the surrounding walls and the bottom of the tank to represent the ambient temperature (see Table 1).

3. Results and discussion

A systematic study on the effects of temperature gradient flow and its impact on the efficiency of serpentine chlorine contact tank, is carried out using the numerical model developed in §2. Eight simulation scenarios were explored to identify and quantify the impact of inflow and ambient temperature on the tracer transport and hydraulic efficiency of the contact tank. 3.1. Hydraulic efficiency of the serpentine contact tank

The spatially-averaged tracer concentration values at the outlet numerical boundaries are computed for each time-step. Fig. 4 and 5 compare the temporal variation of tracer concentration at the outlet of the baffled chlorine contact tank, for the cases with inflow temperature variations (Case No. 1 – 4) and those cases with ambient wall temperature variations (Case No 5 – 8). The results show that the total injected tracer mass pass through the tank outlet in one hour. For the cases with inflow temperature variations, Fig. 4 demon-

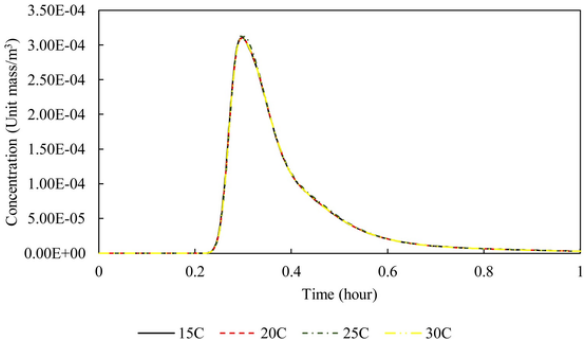

Fig. 4. Residence time distribution curves for simulation scenarios with inflow tempera-

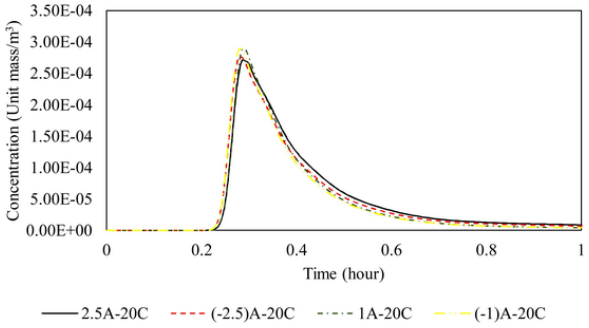

Fig. 5. Residence time distribution curves for the simulation scenarios with constant inflow temperature (= 20 °C) and varying ambient temperature of +2.5 °C, -2.5 °C, +1 °C and -1 °C.

strates that there is no significant differences between RTD curves for inflow temperature of 15 °C, 20 °C, 25 °C and 30 °C and all RTD curves have similar rise, peak and tail. The characteristic dimensionless hydraulic efficiency indexes including; $\theta_{10} = \frac{t_{10}}{\tau}$, $\theta_p = \frac{t_p}{\tau}$, $\theta_{90} = \frac{t_{90}}{\tau}$, $Mo = \frac{t_{90}}{t_{10}}$ are defined by theoretical residence time τ. The hydraulic efficiency indicators of the baffled chlorine contact tank were determined by analyzing residence time distribution (Table 5). The analysis of hydraulic efficiency indexes presented in Table 5 indicates that variation in flow temperature at the inlet (15 °C, 20 °C, 25 °C and 30 °C) has no significant effects on the hydraulic efficiency of the serpentine tanks. The Real Hydraulic Retention Time (HRT_R), effective volume (e), θ_{10}, θ_p, θ_{90} and M_o are shown to remain approximately constant between test case No. 1 – 4 (inflow of 15 °C, 20 °C, 25 °C and 30 °C). The simulation results of the cases No. 1 – 4 can be interpreted as inflow temperature does not significantly influence flow hydrodynamic structure and density of water throughout the serpentine chlorine contact tank.

For the simulation cases with constant inflow temperature (= 20 °C) and ambient wall temperature variations (+2.5 °C, -2.5 °C, +1 °C and -1 °C), the analysis of numerical results presented in Table 5 shows that the hydraulic efficiency of the baffled contact tank was reduced. The effective volume of the tank was reduced by approximately, 10, 12, 4 and 5 percent, for the test cases No. 5 – 8, respectively. The numerical results show that for the cases with lower ambient temperature (Case No. 5 [-2.5 °C] & 7 [-1 °C]), the short-cutting was intensified due to temperature induced stratification inside the baffled contact tank. From the numerical results it can be concluded that lower ambient temperature variations will result in more intensely stratified flow and therefore an accelerated short-cutting condition in the chlorine contact tanks (e.g. case No. 5).

For the simulation scenarios with ambient temperature variations (Case No. 5 – 8), the tracer peak concentration time θ_p was decreased due to reduction in the effective volume of the tank and alteration of flow conditions as a result of intensified short-cutting and mixing throughout the tank. The largest reduction in peak tracer concentration time θ_p as well as drastic reduction in effective volume of the contact tank was occurred for the case No. 5, with the highest ambient temperature (= +2.5 °C) and the most intense flow short-cutting. To determine the mixing characteristics for the serpentine contact tank, Morrill index ($Mo = \frac{t_{90}}{t_{10}}$) was determined for all the simulation scenarios. Table 5 shows an increased mixing for the cases with ambient temperature variations (Scenario No. 5 – 8) in comparison to those scenarios with no wall temperature (Scenario No. 1 – 4), which is mainly influenced by buoyancy flow created by inflow-ambient temperature variation inside the tank.

Table 5
Hydraulic Efficiency Indicators for all the cases.

No.	Case	HRT_R	e	θ_{10}	θ_p	θ_{90}	Mo
–	Experimental study of Angeloudis et al. [28]	N/A	N/A	0.7	0.84	1.48	2.12
1	15C	19.4977	0.92	0.6869	0.8484	1.4801	2.1548
2	20C	19.4977	0.92	0.6869	0.8484	1.4801	2.1548
3	25C	19.4961	0.92	0.6869	0.8484	1.4801	2.1548
4	30C	19.4977	0.92	0.6869	0.8484	1.4801	2.1548
5	2.5A-20C	17.2571	0.82	0.6632	0.8053	1.5159	2.2857
6	(-2.5)A-20C	16.8666	0.80	0.6907	0.8290	1.5789	2.2860
7	1A-20C	18.6134	0.88	0.6656	0.8100	1.5064	2.2633
8	(-1)A-20C	18.4156	0.87	0.6888	0.8266	1.5277	2.2180

3.1. Temperature distribution in the serpentine disinfection tank

The numerical simulations highlight the effects of both inflow and ambient temperature variations on the performance of baffled chlorine tank and development of thermally-induced flow stratification. Fig. 6 depicts the vertical variation of temperature in the flow, for the test cases No. 5 – 8, at the center of all compartments of the baffled chlorine tank. The thermal stratification derived by the difference between ambient and inflow temperature is evident in all the compartments of the contact tank (Fig. 6). A decreasing trend in the intensity of thermal stratification was observed as the water passed through the compartments of the baffled tank. The maximum and the minimum thermal stratification were seen at the first and last compartments of the tank, respectively. The thermal stratification results are in good agreement with previous studies [47,48].

3.2. Effect of temperature on chlorine decay

3.2.1. Temperature effects on the efficiency of the serpentine contact tank

The impacts of inflow (15°, 20°, 25° & 30 °C) and ambient (+2.5 °C, -2.5 °C, +1 °C & -1 °C) temperature variations on the chlorine decay and efficiency of the serpentine disinfection tank is assessed with the three-dimensional advection-diffusion and Reynolds averaged species models implemented in this study. A constant initial chlorine concentration of 2 mg/l was introduced for all simulation cases. The spatially averaged concentration of chlorine at the outlet boundary, were determined for every 25 s of the simulation.

Fig. 7 illustrates the temporal variation of spatially-averaged chlorine concentration at the outlet boundaries of the baffled contact tank for all simulation scenarios (Case No. 1 – 8). The uniform injection of chlorine, into the water at the numerical inlet, was performed for a period of 5000 s until the chlorine concentration was reached a steady and constant value at the outlet boundary. Fig. 8 depicts the depth-averaged chlorine concentration across the baffled contact tank for the cases with inflow temperature variation of 15 °C, 20 °C, 25 °C and 30 °C (Case No. 1 – 4). The figure highlights the significance of inflow (effluent) temperature variation influences on the combined fast and slow chlorine decay processes in the serpentine contact tank. The highest chlorine decay rate was observed for the case of inflow temperature of 30 °C (Case No. 4), followed by the cases of inflow temperature of 25 °C, 20 °C, and the least effects on chlorine decay was observed for the case of inflow temperature of 15 °C (Case No.1).

The spatially-averaged chlorine concentrations at the outlet boundaries were determined after reaching steady-state and it was measured at 1.226, 0.93, 0.79 and 0.49 (mg/l) for the simulation scenario No.1–4, respectively. The analysis of chlorine concentration and decay rates at the outlet of the serpentine contact tank indicates that, a 15 °C increase of inflow (effluent) temperature can result in 37 % reduction in the final chlorine concentration due to the effects of temperature on both fast and slow chlorine decay processes. Table 6 summarizes the initial and final chlorine concentration as well as the decay rates (%) for all of the simulation scenarios (Cases No. 1 – 8).

The effects of ambient temperature on the efficiency of baffled disinfection tanks were investigated with four simulation scenarios (Case No. 5 – 8) where the ambient temperature was set on the surrounding walls and the bottom boundary conditions of the numerical domain, along with a constant inflow temperature (= 20 °C). The findings of the numerical analysis show that ambient temperature has significant impacts on the chlorine decay rate. Fig. 9 illustrates the depth-av-

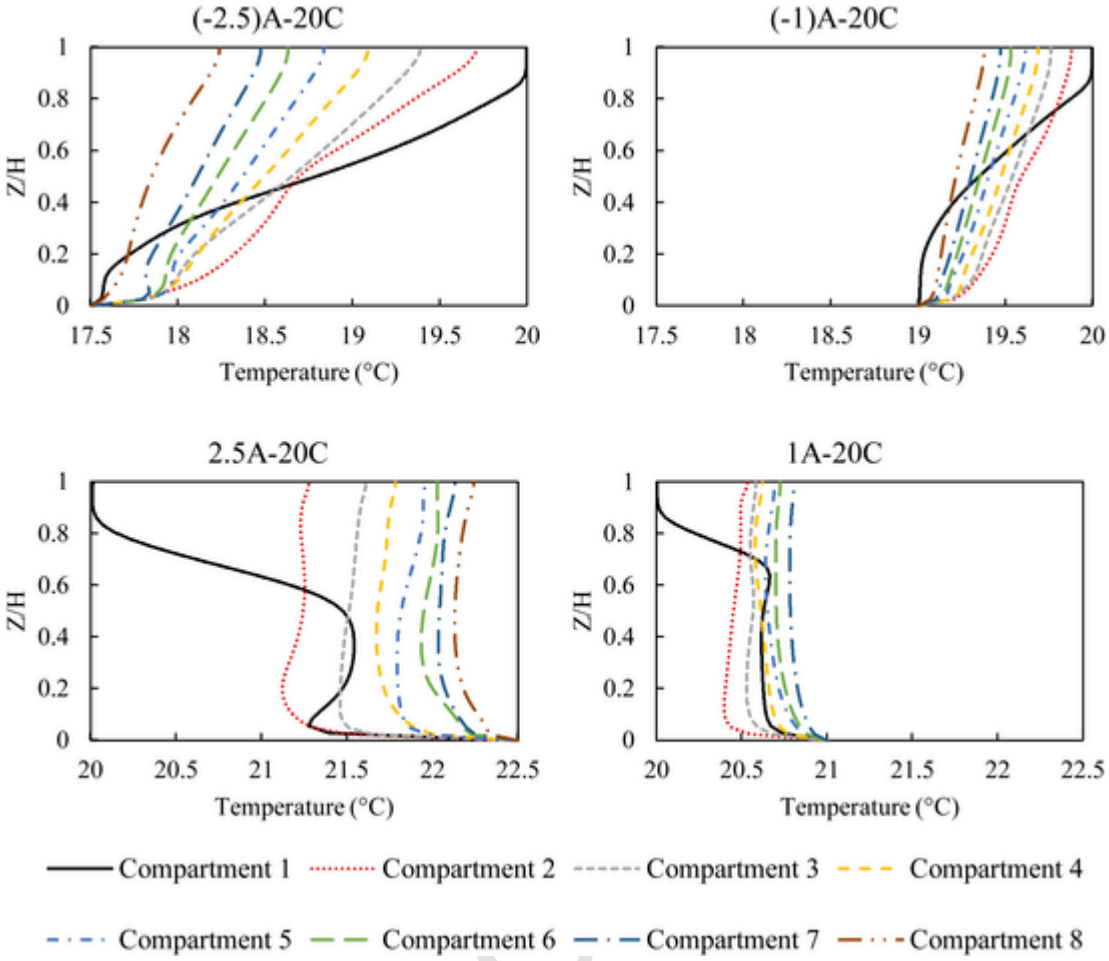

Fig. 6. Vertical temperature profiles for simulation case No. 5 – 8, at the center of all compartments of the baffled contact tank.

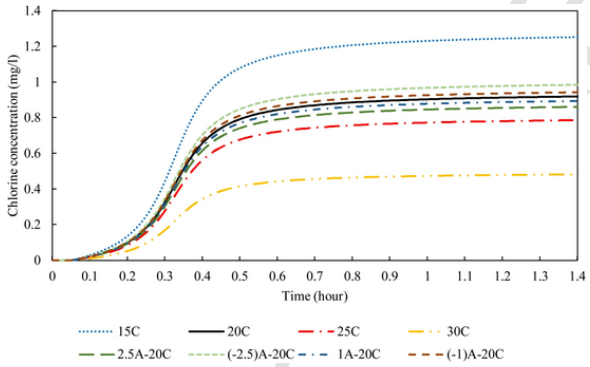

Fig. 7. Temporal variation of spatially-averaged chlorine concentration at the outlet boundary.

fled disinfection tank for the case No. 5 – 8 (see Table 4). The numerical data indicates that increase in ambient temperature accelerate the chlorine decay rates. For the Case No. 5 with +2.5 °C ambient temperature, the buoyancy flow effects were observed in the first chamber of the baffled contact tank. It was shown that an increase of 2.5 °C and 1 °C in ambient temperature, increase chlorine decay by 3.5 % and 2%, respectively. For the test cases No. 5 – 8, with ambient temperature effects, the efficiency of the water disinfection processes in the serpentine chlorine contact tank is significantly influenced by the effects of temperature on hydraulic performance due to flow density and viscosity alterations.

4. Conclusion

This paper developed a robust numerical model for simulating effects of temperature varying flow on the efficiency of water disinfection processes in serpentine chlorine contact tanks. The flow hydrodynamic is modeled using RANS equations in conjunction with $k-\varepsilon$ turbulence closure model. The advection-diffusion equation in the three-dimensional Cartesian coordinate system is implemented in the numerical model to simulate solute transport processes in the tank. The impacts of temperature variations on density and viscosity of the fluid flow is simulated by incorporating Millero and Poisson [21] model and Vogel's equation [22], respectively. Chlorine decay processes are simulated using the Reynolds-averaged species transport model.

The effects of inflow and ambient temperature variations on the hydraulic performance and efficiency of baffled chlorine contact tanks were investigated with the use of the numerical model developed within this study. The model was successfully validated against the physical modelling measurements of Angeloudis et al. (2014). The analysis of numerical results showed that the developed model is capable of robust and efficient prediction of flow characteristics, scalar transport, and temperature effects on the hydraulic efficiency and chlorine concentration decay processes in the baffled contact tanks.

The numerical simulations indicated the significance of inflow (Case No. 1 – 4) and ambient (Case No. 5 – 8) temperature on the overall efficiency of the disinfection process as well as hydraulic efficiency and chlorine decay rates in the baffled tanks. The findings showed a reduction in the hydraulic efficiency of the tank due to buoyancy flow resulted from temperature variations inside the tank. The analysis of numerical simulations indicated that increase in ambient and inflow temperature can increase chlorine decay by up to 75 %, leading to undesirable disinfection consequences and disruption of water treat-

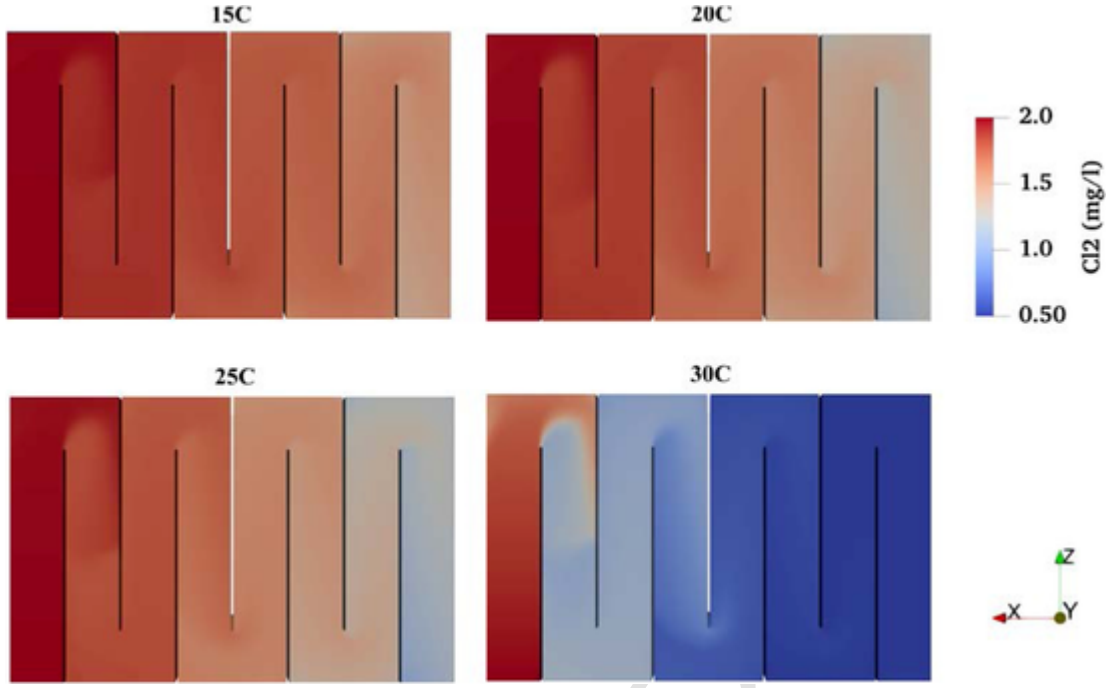

Fig. 8. Depth-averaged Chlorine concentration distribution map for the cases with inflow temperature of 15 °C, 20 °C, 25 °C and 30 °C (Case No. 1 – 4).

Table 6
Precentage of Chlorine decay for the simulation scenarios.

Case	Initial concentration at the inlet (mg/l)	Final concentration at the outlet (mg/l)	Chlorine decay (%)
15C	2	1.26	38
20C		0.93	53
25C		0.79	61
30C		0.49	75
2.5A-20C		0.87	56.5
(-2.5)A-20C		0.99	50.5
1A-20C		0.90	55
(-1)A-20C		0.95	52.5

ment processes. The numerical model developed within this study was shown to be a robust and efficient tool to determine optimum inflow and ambient temperature configurations for high-efficiency water treatment processes to prevent microorganism residual and by-products disinfection formation. The computational framework presented in this study can be used by engineers for the optimum design of water and wastewater treatment processes and chlorine contact tanks with complex geometrical designs such as serpentine tanks. Systematic comparison of different chlorine decay and turbulence models and their impacts on the numerical robustness and accuracy can be done to further optimize the numerical modelling framework outlined in this study.

Declaration of Competing Interest

All the authors of this paper certify that they have NO affiliations with or involvement in any organization or entity with any financial interest (such as honoraria; educational grants; participation in speakers' bureaus; membership, employment, consultancies, stock ownership, or other equity interest; and expert testimony or patent-licensing arrangements), or non-financial interest (such as personal or professional relationships, affiliations, knowledge or beliefs) in the subject matter or materials discussed in this manuscript.

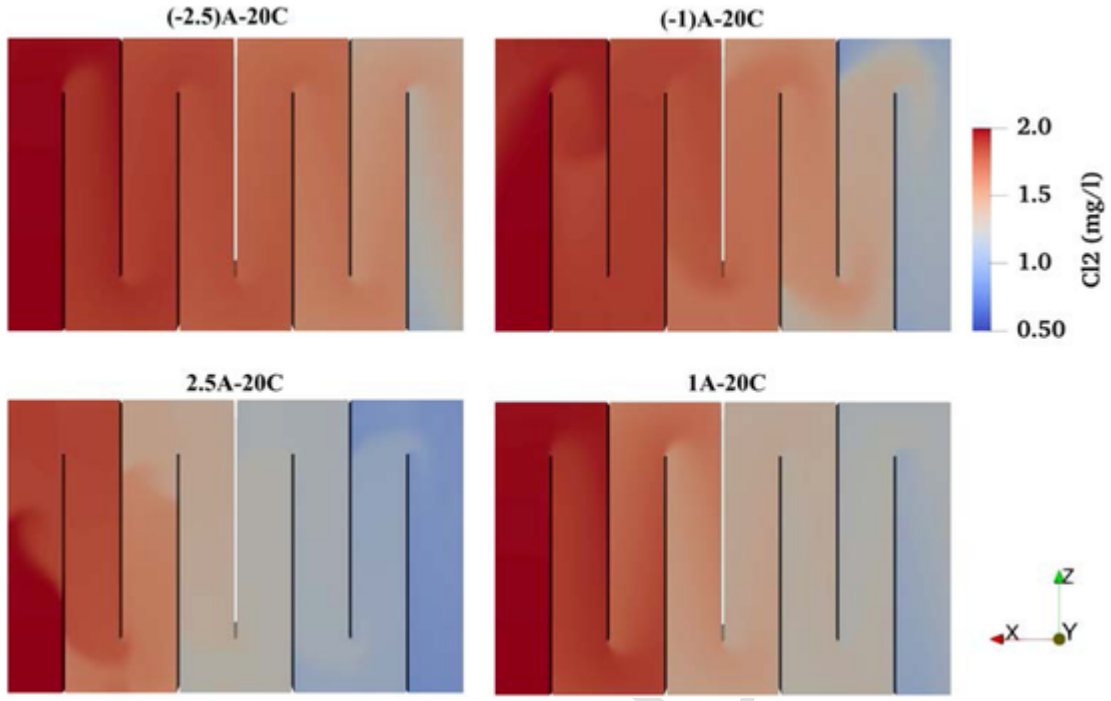

Fig. 9. Depth-averaged Chlorine concentration distribution map for the cases with constant inflow temperature (= 20 °C) and varying ambient concentration of +2.5 °C, -2.5 °C, +1 °C and -1 °C).

References

[1] S Borzooei, R Teegavarapu, S Abolfathi, Y Amerlinck, I Nopens, M C Zanetti, Impact evaluation of wet-weather events on influent flow and loadings of a Water Resource recovery facility, International Conference on Urban Drainage Modelling, Springer, 2018, doi:10.1007/978-3-319-99867-1_122.

[2] S Borzooei, Y Amerlinck, S Abolfathi, D Panepinto, I Nopens, E Lorenzi, L Meucci, M C Zanetti, Data scarcity in modelling and simulation of a large-scale WWTP: stop sign or a challenge, J. Water Process. Eng. 28 (2019) 10–20, doi:10.1016/j.jwpe.2018.12.010.

[3] S Borzooei, R Teegavarapu, S Abolfathi, Y Amerlinck, I Nopens, M C Zanetti, Data mining application in assessment of weather-based influent scenarios for a WWTP: getting the most out of plant historical data, water, air, Water Air Soil Pollut. Focus. 230 (1) (2019) 5, doi:10.1007/s11270-018-4053-1.

[4] B Metcalf, G Eddy, Tchobanoglous. Wastewater Engineering: Treatment Disposal Reuse, Central Book Company, 2014.

[5] F Edition, Guidelines for drinking-water quality, WHO Chron. 38 (4) (2011) 104–108.

[6] J C Powell, N B Hallam, J R West, C F Forster, J Simms, Factors which control bulk chlorine decay rates, Water Res. 34 (1) (2000) 117–126, doi:10.1016/S0043-1354(99)00097-4.

[7] J Menaia, S Coelho, A Lopes, E Fonte, J Palma, Dependency of bulk chlorine decay rates on flow velocity in water distribution networks, Water Sci. Technol. Water Supply 3 (1–2) (2003) 209–214, doi:10.2166/ws.2003.0105.

[8] D Brown, J Bridgeman, J R West, Predicting chlorine decay and THM formation in water supply systems, Rev. Environ. Sci. Biotechnol. 10 (1) (2011) 79–99, doi:10.1007/s11157-011-9229-8.

[9] S Abolfathi, J Pearson, Application of smoothed particle hydrodynamics (SPH) in nearshore mixing: a comparison to laboratory data, Coast. Eng. Proc. 1 (35) (2017) 16, doi:10.9753/icce.v35.currents.16.

[10] S Abolfathi, J Pearson, Solute dispersion in the nearshore due to oblique waves, Coast. Eng. Proc. 1 (34) (2014) 49, doi:10.9753/icce.v34.waves.49.

[11] S Abolfathi, D Shudi, S Borzooei, A Yeganeh-Bakhtiari, J Pearson, Application of smoothed particle hydrodynamics in evaluating the performance of coastal retrofit structures, Coast Eng. Proc (2018), doi:10.9753/icce.v36.papers.109.

[12] A Fitri, R Hashim, S Abolfathi, A Maulud, K Nizam, Dynamics of sediment transport and erosion-deposition patterns in the locality of a detached low-crested breakwater on a cohesive coast, Water. 11 (8) (2019) 1721, doi:10.3390/w11081721.

[13] A Yeganeh-Bakhtiary, H Houshangi, F Hajivalie, S Abolfathi, A numerical study on hydrodynamics of standing waves in front of caisson breakwaters with WCSPH model, Coast. Eng. J. 59 (1) (2017), doi:10.1142/S057856341750005X 1750005-1-1750005-31.

[14] A Yeganeh-Bakhtiary, H Houshangi, S Abolfathi, Lagrangian two-phase flow modeling of scour in front of vertical breakwater, Coast. Eng. J. (2020) 1–15, doi:10.1080/21664250.2020.1747140.

[15] D Goodarzi, K S Lari, A Alighardashi, A large eddy simulation study to assess low-speed wind and baffle orientation effects in a water treatment sedimentation basin, Water Sci. Technol. 2017 (2) (2018) 412–421, doi:10.2166/wst.2018.171.

[16] A. Alighardashi, D. Goodarzi, Simulation of depth and wind effects on the hydraulic efficiency of sedimentation tanks, Water and Environment Journal. https://doi.org/10.1111/wej.12478.

[17] J Zhang, X Xu, A Tejada-Martinez, Q Zhang, E Wicklein, Evaluating reactor hydraulics in a cost-effective and environment-friendly way: numerical tracer study, AWWA Water Science. 1 (6) (2019) e1163, doi:10.1002/aws2.1163.

[18] M M Aral, E Demirel, Novel slot-baffle design to improve mixing efficiency and reduce cost of disinfection in drinking water treatment, J. Environ. Eng. 143 (9) (2017), doi:10.1061/(ASCE)EE.1943-7870.0001266 06017006.

[19] E Demirel, M M Aral, Performance of efficiency indexes for contact tanks, J. Environ. Eng. 144 (9) (2018), doi:10.1061/(ASCE)EE.1943-7870.0001431 04018076.

[20] J Zhang, A Tejada-Martínez, Q Zhang, Reynolds-averaged Navier-Stokes simulation of the flow and tracer transport in a multichambered ozone contactor, J. Environ. Eng. 139 (3) (2012) 450–454, doi:10.1061/(ASCE)EE.1943-7870.0000648.

[21] J Zhang, A Tejada-Martínez, Q Zhang, Hydraulic efficiency in RANS of the flow in multichambered contactors, J. Hydraul. Eng. 139 (11) (2013) 1150–1157, doi:10.1061/(ASCE)HY.1943-7900.0000777.

[22] H Wang, X Shao, R A Falconer, Flow and transport simulation models for prediction of chlorine contact tank flow-through curves, Water Environ. Res. 75 (5) (2003) 455–471, doi:10.2175/106143003X141268.

[23] D Kim, T Stoesser, J-H Kim, The effect of baffle spacing on hydrodynamics and solute transport in serpentine contact tanks, J. Hydraul. Res. 51 (5) (2013) 558–568, doi:10.1080/00221686.2013.777681.

[24] B Wols, J Hofman, W Uijttewaal, L Rietveld, J Van Dijk, Evaluation of different disinfection calculation methods using CFD, Environ. Model. Softw. 25 (4) (2010) 573–582, doi:10.1016/j.envsoft.2009.09.007.

[25] N Nasyrlayev, M A Kizilaslan, A T Kurumus, E Demirel, M M Aral, A perforated baffle design to improve mixing in contact tanks, Water 12 (4) (2020) 1022.

[26] J S Carlston, S K Venayagamoorthy, Impact of modified inlets on residence times in baffled tanks, J. Am. Water Works Assoc. 107 (6) (2015) E292–E300, doi:10.5942/jawwa.2015.107.0078.

[27] J Zhang, A E Tejada-Martínez, Q Zhang, H Lei, Evaluating hydraulic and disinfection efficiencies of a full-scale ozone contactor using a RANS-based modeling framework, Water Res. 52 (2014) 155–167, doi:10.1016/j.watres.2013.12.037.

[28] A Angeloudis, T Stoesser, R A Falconer, Predicting the disinfection efficiency range in chlorine contact tanks through a CFD-based approach, Water Res. 60 (2014) 118–129, doi:10.1016/j.watres.2014.04.037.

[29] M A Kizilaslan, E Demirel, M M Aral, Efficiency enhancement of chlorine contact tanks in water treatment plants: a full-scale application, Processes. 7 (9) (2019) 551, doi:10.3390/pr7090551.

[30] P Ouro, B Fraga, N Viti, A Angeloudis, T Stoesser, C Gualtieri, Instantaneous transport of a passive scalar in a turbulent separated flow, Environ. Fluid Mech. 18 (2) (2018) 487–513, doi:10.1007/s10652-017-9567-3.

[31] J Zhang, A E Tejada-Martínez, Q Zhang, Evaluation of large eddy simulation and RANS for determining hydraulic performance of disinfection systems for water treatment, J. Fluids Eng. 136 (12) (2014), doi:10.1115/1.4027652.

[32] F Long, B Deng, Y Xu, J Gao, Y Zhang, Numerical simulation of the disinfection performance in an annular reactor with different internal configurations, J. Water Process. Eng. 31 (2019), doi:10.1016/j.jwpe.2019.100824 100824.

[33] I Fisher, G Kastl, A Sathasivan, V Jegatheesan, Suitability of chlorine bulk decay models for planning and management of water distribution systems, Crit. Rev. Environ. Sci. Technol. 41 (20) (2011) 1843–1882, doi:10.1080/10643389.2010.495639.

[34] P Roccaro, H-S Chang, F G Vagliasindi, G V Korshin, Differential absorbance study of effects of temperature on chlorine consumption and formation of disinfection

products in chlorinated water, Water Res. 42 (8–9) (2008) 1879–1888, doi:10.1016/j.watres.2007.11.013.
[35] A Angeloudis, Numerical and Experimental Modelling of Flow and Kinetic Processes in Serpentine Disinfection Tanks, Cardiff University, 2014.
[36] S Patankar, Numerical Heat Transfer and Fluid Flow, CRC press, 2018.
[37] P J Roache, Fundamentals of Computational Fluid Dynamics(Book), Hermosa Publishers, Albuquerque, NM, 1998, p. 1998.
[38] H K Versteeg, W Malalasekera, An introduction to computational fluid dynamics: the finite volume method, Pearson Education (2007).
[39] S B Pope, Turbulent Flows, IOP Publishing, 2001.
[40] H Tennekes, J L Lumley, J L Lumley, A First Course in Turbulence, MIT press, 1972.
[41] K Hanjalić, S Kenjeres, M Tummers, H Jonker, Analysis and modelling of physical transport phenomena, VSSD (2007).
[42] T Maric, J Hopken, K Mooney, The OpenFOAM Technology Primer, 2014.
[43] R B Bird, W E Stewart, E N Lightfoot, Transport Phenomena, John Wiley & Sons, 2006.
[44] W Jones, B E Launder, The prediction of laminarization with a two-equation model of turbulence, Int. J. Heat Mass Transf. 15 (2) (1972) 301–314, doi:10.1016/0017-9310(72)90076-2.
[45] A Angeloudis, T Stoesser, C Gualtieri, R A Falconer, Contact tank design impact on process performance, Environ. Model. Assess. 21 (5) (2016) 563–576, doi:10.1007/s10666-016-9502-x.
[46] E Demirel, M Aral, Unified Analysis of Multi-Chamber Contact Tanks and Mixing Efficiency Evaluation Based on Vorticity Field. Part II: Transport Analysis, Water 8 (11) (2016) 537, doi:10.3390/w8110537.
[47] E Hendi, A Y Shamseldin, B W Melville, S E Norris, Experimental investigation of the effect of temperature differentials on hydraulic performance and flow pattern of a sediment retention pond, Water Sci. Technol. 77 (12) (2018) 2896–2906, doi:10.2166/wst.2018.286.
[48] D Goodarzi, K Sookhak Lari, F Mossaiby, Thermal effects on the hydraulic performance of sedimentation ponds, J. Water Process. Eng. 33 (2020), doi:10.1016/j.jwpe.2019.101100 101100.
[49] F J Millero, A Poisson, International one-atmosphere equation of state of seawater, Deep. Sea Res. Part A Oceanogr. Res. Pap. 28 (6) (1981) 625–629, doi:10.1016/0198-0149(81)90122-9.
[50] M L Huber, R A Perkins, A Laesecke, D G Friend, J V Sengers, M J Assael, I N Metaxa, E Vogel, R Mareš, K Miyagawa, New international formulation for the viscosity of H 2 O, J. Phys. Chem. Ref. Data 38 (2) (2009) 101–125, doi:10.1063/1.3088050.
[51] J Zhang, A E Tejada-Martínez, Q Zhang, Developments in computational fluid dynamics-based modeling for disinfection technologies over the last two decades: a review, Environ. Model. Softw. 58 (2014) 71–85, doi:10.1016/j.envsoft.2014.04.003.
[52] C Gualtieri, A Angeloudis, F Bombardelli, S Jha, T Stoesser, On the values for the turbulent Schmidt number in environmental flows, Fluids 2 (2) (2017) 17, doi:10.3390/fluids2020017.
[53] D Kim, T Stoesser, J-H Kim, Modeling aspects of flow and solute transport simulations in water disinfection tanks, Appl. Math. Model. 37 (16–17) (2013) 8039–8050, doi:10.1016/j.apm.2013.03.031.
[54] M Van Reeuwijk, K S Lari, Asymptotic solutions for turbulent mass transfer augmented by a first order chemical reaction, Int. J. Heat Mass Transf. 55 (23–24) (2012) 6485–6490, doi:10.1016/j.ijheatmasstransfer.2012.06.048.
[55] C Gualtieri, Numerical Simulation of Flow and Tracer Transport in a Disinfection Contact Tank, 2006.
[56] E L Thackston, F D Shields Jr., P R Schroeder, Residence time distributions of shallow basins, J. Environ. Eng. 113 (6) (1987) 1319–1332.
[57] J Persson, H B Wittgren, How hydrological and hydraulic conditions affect performance of ponds, Ecol. Eng. 21 (4–5) (2003) 259–269, doi:10.1016/j.ecoleng.2003.12.004.
[58] US EPA, Disinfection Profiling and Benchmarking Guidance Manual, 1999.
[59] E C Teixeira, R do Nascimento Siqueira, Performance assessment of hydraulic efficiency indexes, J. Environ. Eng. 134 (10) (2008) 851–859, doi:10.1061/(ASCE)0733-9372(2008)134:10(851).
[60] C Gualtieri, Discussion of "Performance assessment of hydraulic efficiency indexes" by Edmilson Costa teixeira and Renato do nascimento siqueira, J. Environ. Eng. 136 (9) (2010) 1006–1007, doi:10.1061/(ASCE)EE.1943-7870.0000088.
[61] D Brown, J R West, B J Courtis, J Bridgeman, Modelling THMs in water treatment and distribution systems, Proceedings of the Institution of Civil Engineers-Water Management, Thomas Telford Ltd, 2010, doi:10.1680/wama.2010.163.4.165.
[62] L Monteiro, R M Viegas, D I Covas, J Menaia, Modelling chlorine residual decay as influenced by temperature, Water Environ. J. 29 (3) (2015) 331–337, doi:10.1111/wej.12122.
[63] B J Courtis, J R West, J Bridgeman, Temporal and spatial variations in bulk chlorine decay within a water supply system, J. Environ. Eng. 135 (3) (2009) 147–152, doi:10.1061/(ASCE)0733-9372(2009)135:3(147).
[64] F Hua, J West, R Barker, C Forster, Modelling of chlorine decay in municipal water supplies, Water Res. 33 (12) (1999) 2735–2746, doi:10.1016/S0043-1354(98)00519-3.
[65] I Fisher, G Kastl, A Sathasivan, A suitable model of combined effects of temperature and initial condition on chlorine bulk decay in water distribution systems, Water Res. 46 (10) (2012) 3293–3303, doi:10.1016/j.watres.2012.03.017.
[66] I Fisher, G Kastl, A Sathasivan, Evaluation of suitable chlorine bulk-decay models for water distribution systems, Water Res. 45 (16) (2011) 4896–4908, doi:10.1016/j.watres.2011.06.032.
[67] A Angeloudis, T Stoesser, R A Falconer, D Kim, Flow, transport and disinfection performance in small-and full-scale contact tanks, J. Hydro-Environ. Res. 9 (1) (2015) 15–27, doi:10.1016/j.jher.2014.07.001.
[68] Dong S., Salauddin M., Abolfathi S., Tan Z. H., Pearson J. M., The Influence of Geometrical Shape Changes on Wave Overtopping: a Laboratory and SPH Numerical Study, Coasts, Marine Structures and Breakwaters 2017 (2018), doi:https://doi.org/10.1680/cmsb.63174.1217.
[69] Borzooei S., Amerlinck Y., Panepinto D., Abolfathi S., Nopens I., Scibilia G., Meucci L., Zanetti M. C., Energy optimization of a wastewater treatment plant based on energy audit data: small investment with high return, Environmental Science and Pollution Research (2020), doi:https://doi.org/10.1007/s11356-020-08277-3.